Engineering and Technology Journal e-ISSN: 2456-3358

Volume 11 Issue 02 February-2026, Page No.-8891-8900

DOI: 10.47191/etj/v11i02.12, I.F. – 8.482

Artificial Intelligence-Enhanced Field Oriented Control for Optimized Speed Control of BLDC Traction Motors in Railway

Wahyu Pribadi[1], Ricto Yudi Wicaksono*[2], Darma Arif Wicaksono[3], Wida Yuliar Rezika[4], Fryscha Febryanti Puspitasari[5], Luki Septya Mahendra[6], Moh. Lutfi Yazid[7]

[1,2,3,4,5]Department of Engineering, Madiun State Polytechnic, Madiun, Indonesia

[6]Department of Industrial Electrical Engineering, Electronic Engineering Polytechnic Institute of Surabaya, Surabaya, Indonesia

[7]Department of Quality Control, PT. INKA, Madiun, Indonesia

ABSTRACT: Brushless Direct Current (BLDC) motors are widely employed in electric railway traction systems due to their high efficiency and smooth operation. However, complex speed control and the occurrence of torque ripple-arising from speed instability under excessive load-prevent BLDC motors from operating at optimal performance. This study proposes an optimization approach based on Field-Oriented Control (FOC) using Proportional Integral (PI) controllers tuned through Hand Tuning (HT), Artificial Bee Colony (ABC), and Particle Swarm Optimization (PSO). The optimization process utilizes the Integral Time Multiplied by Absolute Error (ITAE) criterion. Simulation results indicate that PSO delivers the most optimal overall performance. PSO achieves the highest electromagnetic torque output (26.3937 Nm during start-up and 4.92347 Nm under load), provides the fastest speed recovery, and demonstrates superior resilience to load disturbances such as cornering effects. Therefore, PSO emerges as the most effective tuning strategy for BLDC motor control.

KEYWORDS: Artificial Bee Colony, Field Oriented Control, Hand Tuning, ITAE, BLDC Motor, Particle Swarm Optimization

I. INTRODUCTION

Technological advancement has entered a new phase, known as Society 5.0, characterized by the deep integration of digital technologies [1]. The advent of Industry 5.0 necessitates comprehensive adaptation across all sectors to ensure the production of sophisticated, high-quality products aligned with the needs of society [2]. In the railway sector, digital technologies facilitate sustainable innovation that supports the future development of railway operations [3]. A train is a transportation system composed of a locomotive and multiple carriages, designed to transport large volumes of passengers or freight simultaneously [4]. One of the train types still in operation today is the electric train, which employs electric motors as its main traction system, receiving power directly from the Overhead Line Equipment (OLE) via a pantograph [5].

The Direct Current (DC) motor is a type of traction motor used in electric trains, functioning by converting electrical energy into mechanical rotational motion, and is known for its high initial torque [6]. However, the use of DC motors in electric trains leads to increased noise, as the brushes and commutator create mechanical friction and produce non-smooth rotational motion [7]. Therefore, an improvement is needed, namely the adoption of BLDC motors, which are highly suitable for electric vehicles. A Brushless Direct Current (BLDC) motor operates without brushes and instead relies on electronic commutation, resulting in smoother motor rotation and significantly lower noise levels compared to conventional DC motors [8]. The operating principle of a BLDC motor is based on receiving a DC power supply that is subsequently converted into AC voltage using a DC–AC inverter to drive the motor [9]. However, this technique presents several challenges, including more complex speed regulation and the presence of torque ripple caused by speed instability under excessive load conditions, which prevents the BLDC motor from operating at optimal performance [10].

Therefore, speed regulation can be implemented using the Field-Oriented Control (FOC) method. FOC is a control technique in which a coupled system is transformed into a decoupled system through the orientation of the motor's magnetic field [11]. The FOC method functions by precisely controlling the stator current components of the BLDC motor to achieve accurate torque and speed regulation [12], [13]. The use of the FOC method enables independent control of flux and torque, allowing speed regulation to be managed effectively while reducing the amount of battery power converted into flux [14].

The implementation of a Proportional–Integral (PI) controller for speed regulation in a Field-Oriented Control (FOC) system relies heavily on the optimal tuning of the proportional (K_p) and integral (K_i) gains. Conventional tuning methods, such as manual trial-and-error approaches, often fail to achieve the dynamic response and stability required for electric vehicle applications, particularly when subjected to varying load conditions [15]. To address these challenges, advanced metaheuristic optimization techniques are employed. Specifically, Particle Swarm Optimization (PSO), inspired by the collective behaviour of fish schools and bird flocks, is utilized to determine the optimal parameters that minimize performance indices such as the Integral Time Multiplied by Absolute Error (ITAE). This intelligent control approach is adopted to reduce torque ripple, settling time, and overshoot [16]. The Artificial Bee Colony (ABC) algorithm is proposed as a metaheuristic approach that operates in the same way as PSO, aiming to generate the optimal K*p* and K*i* parameters and ensure robust and stable speed control that overcomes the instability issues typically found in conventionally tuned PI controllers [17].

From the above background, this study proposes a speed control optimization method for Brushless Direct Current (BLDC) motors using Field-Oriented Control (FOC). The system evaluates three tuning approaches are Hand Tuning, Artificial Bee Colony (ABC), and Particle Swarm Optimization (PSO). A Proportional–Integral (PI) controller is employed as the primary control strategy.

II. METHOD

A. *Brushless Direct Current Motor*

BLDC motor control typically relies on techniques that regulate rotor speed and position by adjusting current signals through signal processing and the Space Vector Pulse Width Modulation (SVPWM) method. The current supplied to the motor is controlled based on feedback from rotor speed and position to ensure that the desired torque and speed are achieved.

The initial stage in BLDC motor control is speed regulation, which is performed using a Proportional–Integral (PI) controller. This controller functions to minimize the error (e) between the reference speed (ω_{ref}) and actual speed as expressed in Equation (1).

$$e(t) = \omega_{ref} - \omega_{actual} \quad (1)$$

The PI controller computes the quadrature reference current signal $\left(i_q^{ref}\right)$ which is required to generate the desired torque and speed. This signal is then fed into the inner current loop. The controller output is governed by the standard PI equation in the time domain:

Table 1. Parameters of Inspection Train

Parameter	Value	Unit
Train Mass	200	kg
Maximum Speed	12	km/h
Wheel Diameter	0.26	m
Total Passenger Weight	365	kg

Table 2. Parameters of BLDC Motor BM1424ZXF

Parameter	Value	Unit
Read Output Power	1500	W
Rated Voltage	48	VDC
Rated Speed	2850	Rpm
No Load Speed	3700	Rpm
Full Load Current	31,5	A
No Load Current	5,5	A
Rated Torque	5,026	N.m
Efficiency	82	%
Pole Pairs	5	
Kt (rms)	0,1596	N.m/A
Ke	0,1596	V.s/rad
R_phase	0,1106	Ω
L_phase	0,001	H
J (inertia)	0,010	$Kg.m^2$
B (viscous damping)	0,001	N.m.s/rad

$$u(t) = K_p e(t) + K_i \int e(t)dt \quad (2)$$

The BLDC motor employed in this study is the BM1424ZXF model, which is capable of delivering up to 1500 W of output power. A comprehensive overview of the motor specifications used in the system is provided in Table 2. The BLDC motor type is commonly used in mini train applications. The parameters associated with the mini train system are summarized and presented in Table 1.

B. *Field Oriented Control*

The FOC computation process begins with the control switching into the inner current loop and requires the transformation of the measured three-phase current (i_a, i_b, i_c) into the synchronous dq reference frame. This is achieved through the Clarke Transformation, which convertsi_{abc} into two stationary components (i_α, i_β), followed by the Park Transformation, which uses the rotor angle (θ) to change the $i_{\alpha\beta}$ to be i_d (flux) and i_q (torque). The Park Transformation is defined as follows.

$$\begin{pmatrix} i_d \\ i_q \end{pmatrix} = \begin{pmatrix} cos(\theta) & -sin(\theta) \\ sin(\theta) & cos(\theta) \end{pmatrix} \begin{pmatrix} i_\alpha \\ i_\beta \end{pmatrix} \quad (3)$$

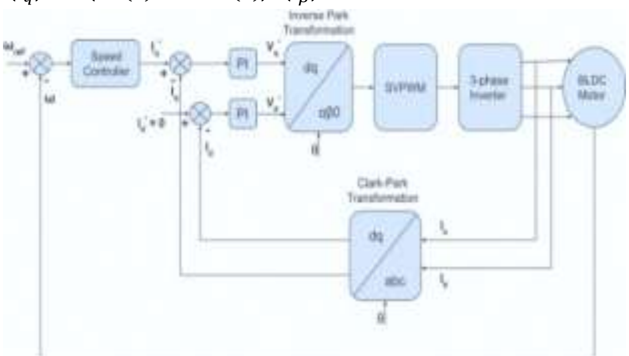

Figure 1. FOC System Block Diagram for BLDC Motor

The value of i_d and i_q measured values are then compared with their respective references (i_d^{ref} and i_q^{ref}). The resulting current error is minimized by the inner-loop PI controllers dedicated to the d- and q-axes, which generate the reference voltages (V_d^{ref} dan V_q^{ref})that are needed by inverter. The q-axis voltage output is formulated as follows

$$V_{qs}^{ref} = K_p I\left(i_q^{ref} - i_q\right) + K_i I \int \left(i_q^{ref} - i_q\right) dt \quad (4)$$

Finally, these reference voltages are transformed back to the stationary three-phase frame through the Inverse Park and Inverse Clarke Transformations, providing the required signals for the SVPWM modulator to efficiently control the three-phase inverter. The Inverse Park Transformation for the voltages is given by,

$$\begin{pmatrix} V_\alpha \\ V_\beta \end{pmatrix} = \begin{pmatrix} cos(\theta) & -sin(\theta) \\ sin(\theta) & cos(\theta) \end{pmatrix} \begin{pmatrix} V_{ds}^{ref} \\ V_{qs}^{ref} \end{pmatrix} \quad (5)$$

The block modeling of the FOC system based on reference [18] is as follows.

C. Hand-Tuning

Manual Tuning, also known as the Trial-and-Error method, is the most traditional and commonly used approach for determining the gain parameters of a PID (Proportional-Integral-Derivative) controller, including the K_p and K_i parameters. This method relies heavily on the intuition and direct observations of the operator or engineer regarding the system's dynamic response. Although it can be used to determine the PI controller constants, it requires extensive understanding of control systems, and its implementation is carried out manually [19].

D. Artificial Bee Colony

The Artificial Bee Colony (ABC) algorithm is a swarm-intelligence–based optimization method that has proven to be effective in finding optimal solutions for complex problems. The algorithm is modeled after the natural foraging behavior of honey bees in locating optimal food sources. ABC is characterized by its minimal control parameters, fast convergence rate, clear logic, and strong exploration–exploitation capabilities. The foraging process is divided into three types of bees: Employed Bees, Onlooker Bees, and Scout Bees [17]. The use of this algorithm begins with the initialization phase. Food sources$\left(x_i^j\right)$ are generated randomly within the specified boundaries (x_{min}^j and x_{max}^j). The second phase, the Employed Bee phase, involves each employed bee searching for a new food source $\left(v_{ij}\right)$ in the neighbourhood of its current food source$\left(x_{ij}\right)$. The position update equation is formulated as follows.

$$v_{ij} = x_{ij} + \emptyset_{ij}\left(x_{ij} - x_{kj}\right) \quad (6)$$

$\emptyset_{ij}$ is a random number, and x_{kj} is the solution selected for exploration. In the next phase, the Onlooker Bees choose food sources to exploit based on a probability (pi) that is proportional to the fitness value (fit_i) of each food source, which is defined as follows:

$$p_i = \frac{fit_i}{\sum_{i=1}^{SN} fit_i} \quad (7)$$

The Scout Bee phase serves as the final stage, in which these bees search for new solutions randomly when a food source has been abandoned (i.e., when the limit is exceeded). Any food source that shows no improvement over a specified number of iterations is considered unproductive and is discarded. This tuning method is applied to the BLDC motor under the FOC scheme to ensure optimal operation.

E. Particle Swarm Optimization

PSO is an advanced optimization algorithm inspired by swarm [20]. The PSO algorithm simulates the social behaviour of animals such as birds and fish. These flocks exhibit cooperative behaviour by using their individual intelligence while also being influenced by the collective behaviour of the group in searching for food. When one bird discovers the correct path or the shortest route to a food source, the other members of the group can immediately follow that path, even if they are located far apart within the flock [21]. A swarm is considered as a group of particles with a defined size, and the initial position of each particle is randomly distributed within a multidimensional search space. Each particle in the swarm adjusts its movement based on two main factors: its own best experience (personal best) and the global best experience of the swarm (global best). If the global best position provides a better result than the particle's current position, the particle will move toward that position through velocity and position updates, as expressed in the following equations.

$$V_i^{(t+1)} = w \times V_i^{(t)} + c_1 r_1\left(pbest_i - X_i^{(t)}\right) + c_2 r_2\left(gbest_i - X_i^{(t)}\right) \quad (8)$$

$$X_i^{(t+1)} = X_i^{(t)} + V_i^{(t+1)} \quad (9)$$

Here, xi(t) represents the position of the i-th particle at iteration ke-t, while vi(t) denotes its velocity. The Parameter w known as the inertia weight, functions to control the balance between exploration and exploitation. The coefficient c_1 is the cognitive coefficient that governs the contribution of the individual experience, whereas c_2 is the social coefficient that governs the contribution of the global experience. The random factors r_1 and r_2 are uniformly distributed numbers within [0,1] providing diversity in the swarm's movement. Through this mechanism, the particles collectively search for the optimal solution within the search space.

F. Integral Time Absolute Error

ITAE emphasizes the error that occurs over time. By multiplying the absolute error($|e(t)|$) by time (t), ITAE assigns increasingly greater weight to errors that occur toward the end of the system response (i.e., after the setpoint has been reached). Its goal is to ensure that the system response not only reaches the setpoint quickly, but also stabilizes rapidly with minimal steady-state error, while heavily penalizing overshoot or prolonged oscillations [22]. The general ITAE expression is defined as follows:

$$ITAE = \int_0^\infty t|e(t)|dt \quad (10)$$

Table 3. Parameters Input

Parameter	Value	Unit
Gear Ratio	7:30	(7 on motor : 30 on train wheel)
Curve Radius	30	m
Curve Angle	97	°
	1.692	rad
Number of Curves	4	

G. Train Track and Simulation Model

The track and simulation model is used to simulate the movement of the train based on the actual track. The simulated train track is illustrated as shown in Figure 2. In real conditions, the track has four curves, each with a different turning duration. Therefore, this needs to be modeled using several mathematical models. To determine the travel distance while turning, Equation (11) can be used as follows.

$$s = r \times \theta \quad (11)$$

Where s is the travel distance, r is the curve radius, and θ is the turning angle. Next, the angular speed of the wheel is calculated using Equation (12).

$$\omega\_wheel = \frac{v}{r\_wheel} \quad (12)$$

Where *ω_wheel* is the angular speed of the wheel, *v* is the train speed when passing through the curve, and *r_wheel* is the wheel radius. Then, to calculate the gear ratio, Equation (13) is used as follows:

$$i = \frac{30}{7} \quad (13)$$

Where *i* is the gear ratio, 30 is the gear ratio on the wheel, and 7 is the gear ratio for the motor. Then, to calculate the motor's angular speed, Equation (14) is used as follows:

$$\omega\_motor = i \times \omega\_wheel \quad (14)$$

Where *ω_motor* is the motor's angular speed, *i* is the gear ratio, and ω_wheel is the wheel's angular speed. In calculating the force and load torque, the centripetal acceleration is required using Equation (15) as follows:

$$a_c = \frac{v^2}{r} \quad (15)$$

Where a_c is the centripetal acceleration, *v* is the train speed when passing through the curve, and *r* is the curve radius. Next, to calculate the centripetal force, Equation (16) is used as follows:

$$F_c = m \times a_c \quad (16)$$

Where F_c is the centripetal force, *m* is the total mass of the train and passengers, and a_c is the centripetal acceleration. Then, to calculate the load torque on the wheel, Equation (17) is formulated as follows:

$$T\_wheelload = F_c \times r\_wheel \quad (17)$$

Where *T_wheelload* is the load torque on the wheel, F_c is the centripetal force, and *r_wheel* is the wheel radius. Then, to calculate the torque on the motor, Equation (18) is expressed as follows:

$$T\_motor = \frac{T\_wheelload}{i} \quad (18)$$

Where *T_motor* is the motor torque, *T_wheelload* is the load torque on the wheel, and *i* is the gear ratio. Then, to calculate the input gain, Equation (19) is used as follows:

$$T_{load} = T\_motor - \Delta\tau \quad (19)$$

Where T_{load} is the input gain, *T_motor* is the motor torque, and $\Delta\tau$ is the torque reduction of the motor. Several input parameters included in Equations (11) to (19) are described in Table 3 parameter input.

III. RESULT AND DISCUSSION

The overall system used in this study is shown in Figure 1, which presents the FOC Block Diagram for the BLDC Motor. As previously discussed, the simulation was conducted using four curvature segments, as illustrated in Figure 2, with Figure 3 serving as a supporting reference. Based on the calculations in Equations (11) through (19), using the input parameters listed in Table 3, the resulting torque–reduction gain values were obtained and are summarized in Table 4. Hence, according to Table 4, curves 1, 2, 3, and 4 have the gain in torque resulting from navigating a curved track of 4.4, 3.8, 4.4, and 4.4, respectively.

The results of this research consist of two main parts. The first part shows the performance of the BLDC motor for the train under no-load conditions. The second part presents the motor behavior when passing through curves with a radius of 30 meters at four different curve points. The second set of results provides a comparison of the current response, electromagnetic torque, and speed using PI controllers tuned with HT (Hand Tuning), ABC tuning, and PSO tuning. The curvature profile for the second condition is shown in Figure 2.

Table 4. Torque Drop Gain Output

Turn	Speed (km/h)	Speed (m/s)	Motor Torque (Nm)	Gain Input (Nm)
1	9,97	2,77	4,4	4,4
2	10,78	2,99	5,13	3,8
3	9,98	2,77	4,4	4,4
4	9,97	2,77	4,4	4,4

Figure 2. the curvature profile of the second condition

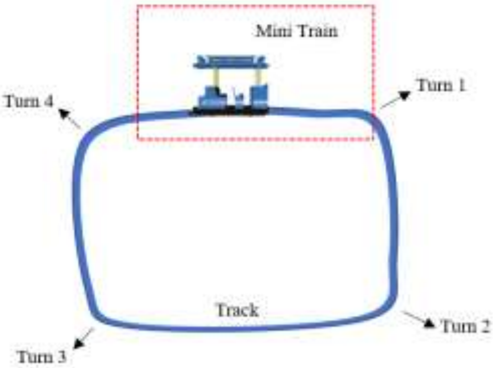

Figure 3. Track Design

The first simulation was performed under no-load conditions. For the speed controller, the HT method yielded Kp = 2 and Ki = 0.1, while the ABC and PSO optimizations produced Kp = 2.1164, and Kp = 2.5138, Ki = 0.0014, respectively. The resulting speed responses for the HT, ABC, and PSO-based FOC schemes are shown in Figures 5–7.

Figure 4 illustrates the inverter current supplying the BLDC motor. Despite the absence of load, a significant inrush current appears during startup, reaching 78.9878 A. After the motor stabilizes, the simulated vehicle is assumed to encounter four track curves with a 30 m radius. Each curvature event produces a distinct rise in current due to increased torque demand.

The first curvature causes the current to increase from 0.2633 A to 30.6975 A between 5.83 s and 10.94 s, followed by a drop to 0.8536 A at 17.87 s. The second curvature produces a peak of 26.6341 A at 21.99 s before decreasing to 0.8546 A at 31.89 s. The third curvature results in a peak of 30.8657 A at 37.04 s and a subsequent decline to 0.8667 A at 43.94 s. The final curvature similarly raises the current to 30.8776 A at 49.04 s, which then returns to 0.8702 A at 54.15 s.

Overall, the current profile demonstrates the motor's dynamic response to curvature-induced load variations despite an initially unloaded condition.

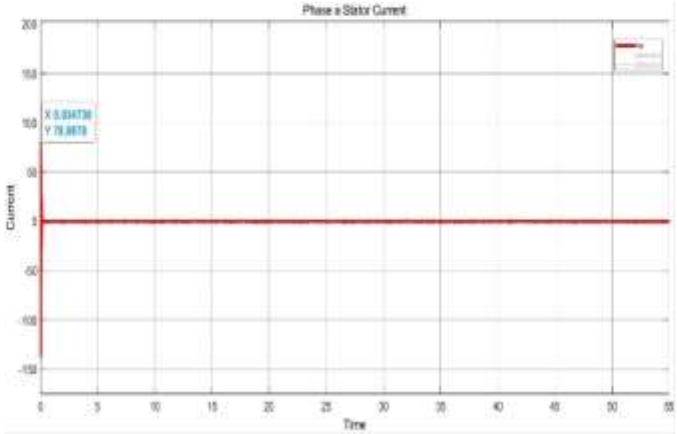

Figure 4. Phase a Stator Current without Load

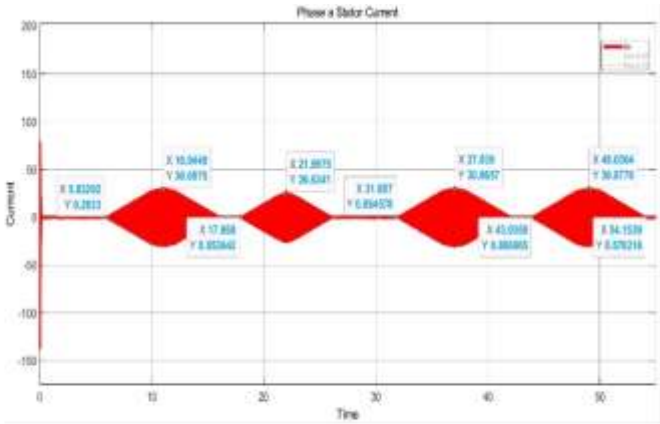

Figure 5. Phase a Stator Current with Load

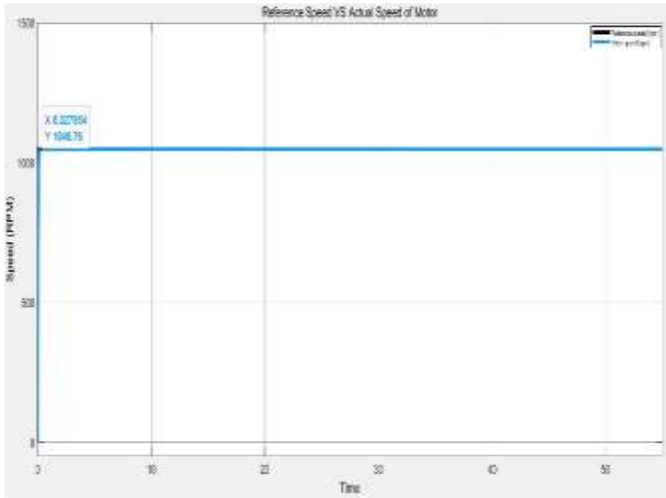

Figure 6. Reference Speed vs Actual Speed of Motor with HT Non-Load

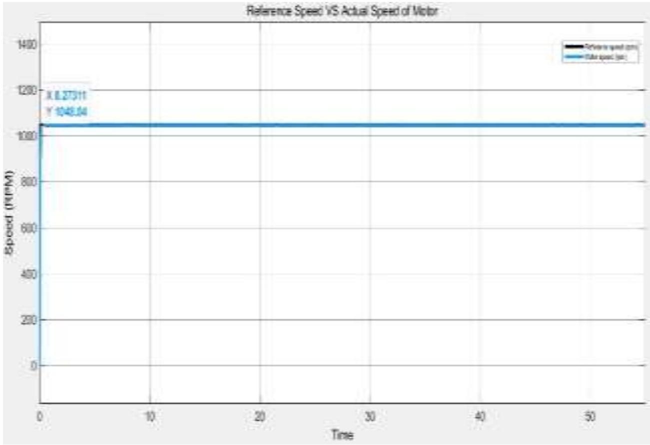

Figure 7. Reference Speed vs Actual Speed of Motor with ABC Non-Load

Figure 6 shows that the HT-based controller achieves a rise time of 0.327954 s, while the ABC-tuned controller in Figure 7 yields a faster rise time of 0.27311 s. In contrast, the PSO-tuned controller shown in Figure 8 produces a rise time of 0.364686 s. These variations in rise time influence how effectively each method responds to torque disturbances.

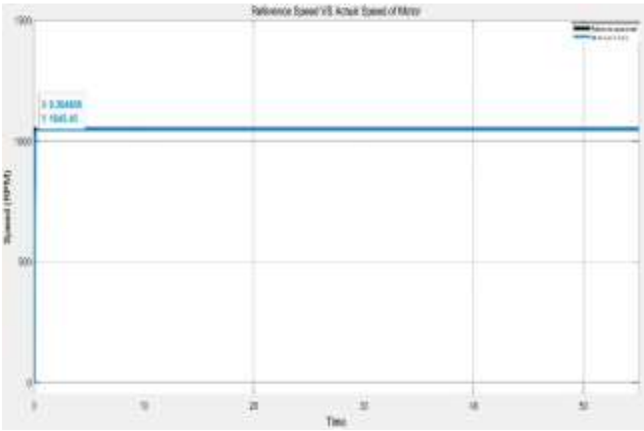

Figure 8. Reference Speed vs Actual Speed of Motor with PSO Non-Load

In this study, torque disturbances are introduced through simulated increases in mechanical load caused by track curvature. The train mass is kept constant, and the additional load arises solely from the torque required to negotiate the curves. The corresponding speed responses for the HT, ABC, and PSO methods are presented in Figures 9, 10 and 11. Each tuning method exhibits distinct dynamic characteristics and advantages under varying load conditions.

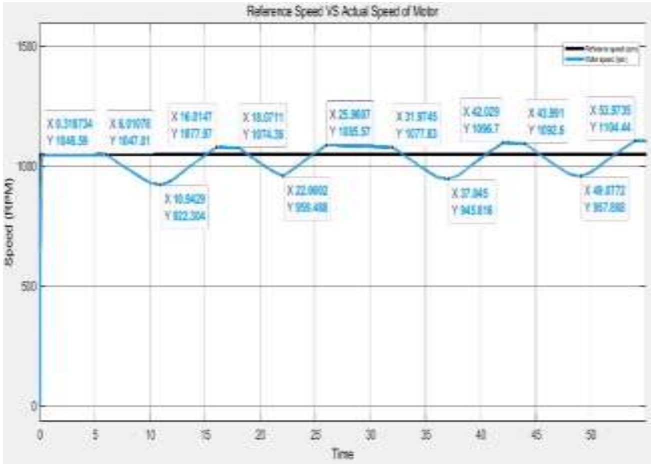

Figure 9. Reference Speed vs Actual Speed of Motor with HT and Load

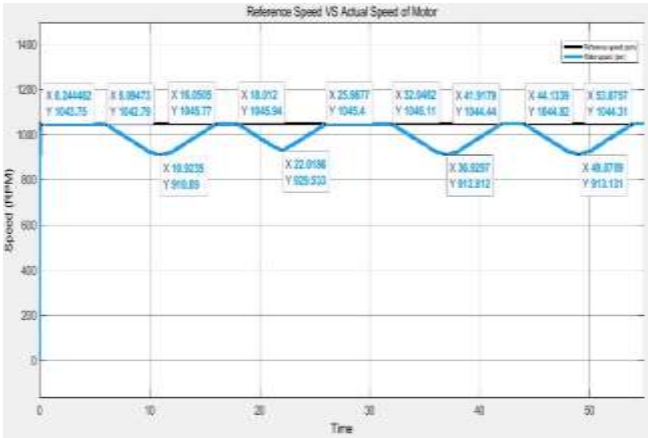

Figure 10. Reference Speed vs Actual Speed of Motor with ABC and Load

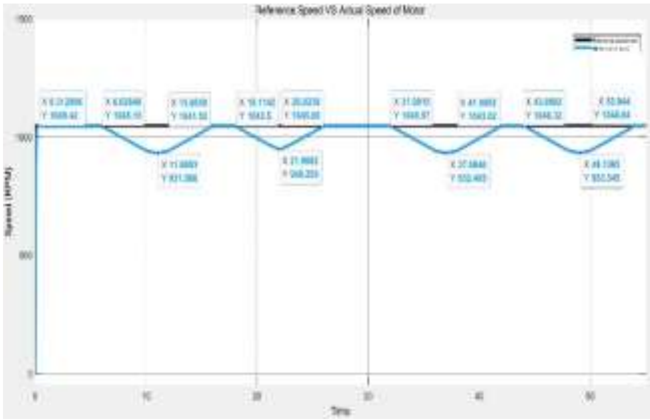

Figure 11. Reference Speed vs Actual Speed of Motor with PSO and Load

Figure 9 shows the FOC configuration implemented using the HT method. In this approach, the proportional and integral gains (K_p and K_i) are yielding Kp = 2 and Ki = 0.1. During this stage, the train experiences a speed reduction as it enters a curved segment, resulting in a rise time of 0.318734 s. The first speed drop occurs at 6.01078 s, where the speed decreases from 1047.01 rpm to 922.304 rpm, followed by recovery at 16.0147 s. Another speed reduction is observed at 18.0711 s, decreasing from 1074.36 rpm to 959.488 rpm, with recovery occurring at 1085.57 s. A subsequent drop takes place at 31.9745 s from 1077.63 rpm to 945.816 rpm, followed by an increase at 42.029 s. The final reduction occurs at 43.991 s, where the speed decreases from 1092.6 rpm to 957.868 rpm, returning to its nominal value at 53.9735 s.

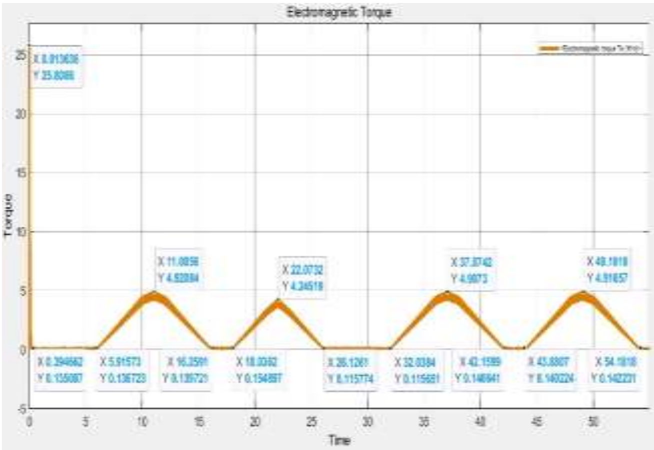

Figure 12. Electromagnetic Torque with HT

Figure 10 illustrates the speed response under load using the ABC method. In this method, the proportional and integral gains (K_p and K_i) are set to 2.1164 and 0.0033, respectively. The resulting rise time is 0.244482 s. The first speed reduction occurs at 6.09473 s, where the speed decreases from 1042.79 rpm to 910.89 rpm, followed by recovery at 16.0505 s. A subsequent drop is observed at 18.012 s, with the speed decreasing from 1045.94 rpm to 929.533 rpm and recovering at 25.9877 s. Another reduction occurs at 32.0462 s, from 1046.11 rpm to 912.812 rpm, with recovery at 41.9179 s. The final speed drop takes place at 44.1339 s, decreasing from 1044.82 rpm to 913.131 rpm, followed by an increase at 53.8757 s.

Figure 11 shows the FOC using the PSO method. In this method, the K_p and K_i values are also calculated based on the ITAE value. According to the PSO, the K_p and K_i values are 2.5138 and 0.0014. When a load is applied, the speed response changes with a rise time of 0.312998 s. A decrease occurs at the first curve at 6.02848 s, where the speed drops from 1045.15 rpm to 931.986 rpm and returns at 15.8638 s. Then, it decreases again at 18.1142 s from 1043.5 rpm to 948.255 rpm and rises again at 26.0238 s. The motor speed decreases again at 31.9915 s from 1045.97 rpm to 932.485 rpm and rises again at 41.9002 s. Then, it decreases once more at 43.8902 s from 1046.32 rpm to 933.345 rpm and rises again at 53.944 s.

In Figures 12, 13, and 14, the electromagnetic torque representation of all methods is shown. At startup, the HT method produces a torque of 25.8086 Nm, while the ABC and PSO methods produce torques of 26.1154 Nm and 26.3937 Nm, respectively. It can be seen that the smallest electromagnetic torque value occurs in the HT method. The highest torque increase when the train passes through a curve occurs in the PSO method, with a value of 4.92347 Nm at 11.0223 s.

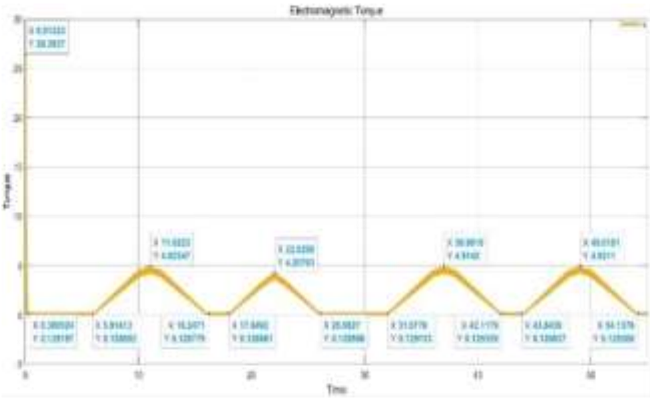

Figure 13. Electromagnetic Torque with PSO

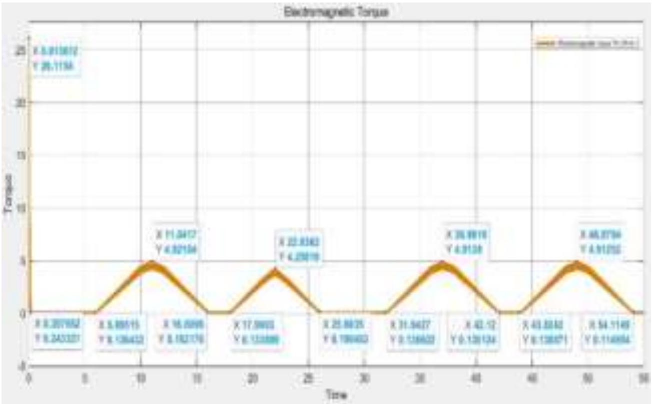

Figure 14. Electromagnetic Torque with ABC

Table 5. The Result of PI-Tuning in All Methods for Speed

Type	Kp	Ki	Rise Point Time	Start Fall Point		Maximum Speed Fall Point		Speed Rise Back Point		Condition
				Time	Speed	Time	Speed	Time	Speed	
HT	2	0.1	0.327954 s	-	-	-	-	-	-	No Load
			0.318734 s	6.01078 s	1047.01 Rpm	10.9429 s	922.304 Rpm	16.0147 s	1077.97 Rpm	Load 1
				18.0711 s	1074.36 Rpm	22.0602 s	959.488 Rpm	25.9607 s	1085.57 Rpm	Load 2

				31.9745 s	1077.63 Rpm	37.045 s	945.816 Rpm	42.029 s	1096.7 Rpm	Load 3
				43.991 s	1092.6 Rpm	49.0772 s	957.868 Rpm	53.9735 s	1104.44 Rpm	Load 4
ABC	2.1164	0.0033	0.27311 s	-	-	-	-	-	-	No Load
			0.244482 s	6.09473 s	1042.79 Rpm	10.9235 s	910.89 Rpm	16.0505 s	1045.77 Rpm	Load 1
				18.012 s	1045.94 Rpm	22.0186 s	929.533 Rpm	25.9877 s	1045.4 Rpm	Load 2
				32.0462 s	1046.11 Rpm	36.9297 s	912.812 Rpm	41.9179 s	1044.44 Rpm	Load 3
				44.1339 s	1044.82 Rpm	49.0709 s	913.131 Rpm	53.8757 s	1044.31 Rpm	Load 4
PSO	2.5138	0.0014	0.364686 s	-	-	-	-	-	-	No Load
			0.312998 s	6.02848 s	1045.15 Rpm	11.0893 s	931.986 Rpm	15.8638 s	1041.52 Rpm	Load 1
				18.1142 s	1043.5 Rpm	21.9682 s	948.255 Rpm	26.0238 s	1045.69 Rpm	Load 2
				31.9915 s	1045.97 Rpm	37.0846 s	932.485 Rpm	41.9002 s	1043.02 Rpm	Load 3
				43.8902 s	1046.32 Rpm	49.1365 s	933.345 Rpm	53.944 s	1048.04 Rpm	Load 4

Table 6. The Result of PI-Tuning in All Methods

Type	Kp	Ki	Start Rising Point		Maximum Surge When Loaded		Condition
			Time	Torque	Time	Torque	
HT	2	0.1	0.013636 s	25.8086 Nm	11.0856 s	4.92084 Nm	Load 1
					22.0732 s	4.24519 Nm	Load 2
					37.0742 s	4.9073 Nm	Load 3
					49.1018 s	4.91657 Nm	Load 4
ABC	2.1164	0.0033	0.013612 s	26.1154 Nm	11.0417 s	4.92104 Nm	Load 1
					22.0362 s	4.25819 Nm	Load 2
					36.9819 s	4.9139 Nm	Load 3
					48.9794 s	4.91252 Nm	Load 4
PSO	2.5138	0.0014	0.01353 s	26.3937 Nm	11.0223 s	4.92347 Nm	Load 1
					22.0298 s	4.25703 Nm	Load 2
					36.9919 s	4.9142 Nm	Load 3
					49.0181 s	4.9211 Nm	Load 4

Table 5 represents several tuning methods based on ITAE that are used for speed control in units of rpm and time in seconds. Among the three tuning methods (HT, ABC, and PSO), the fastest rise time response is obtained by the ABC method with a time of 0.244482 s. The earliest point when the train begins to enter a curve also occurs in the ABC method, with the first curve at 10.9235 s, the second curve at 22.0186 s, the third curve at 36.9297 s, and the fourth curve at 49.0709 s. In addition, the GA method is the method that has the highest speed drop, reaching 910.89 rpm from the stable point or speed reference of 1049 rpm.

At the turnaround point where the speed reaches the reference value, the fastest return time occurs when using the HT method, with 16.0147 s at the first curve, 25.9607 s at the second curve, 42.029 s at the third curve, and 53.9735 s at the fourth curve. However, the speed obtained using HT exceeds the reference speed at each curve. Then, Table 6 represents the electromagnetic torque (Nm) using several FOC techniques. The PSO method has the fastest starting speed, reaching 0.01353 s, and it is also the method with the highest torque, reaching 26.3937 Nm. In addition, the PSO method has the highest torque peak caused by the train passing through a curve, reaching 4.92347 Nm at 11.0223 s on the first curve.

V. CONCLUSIONS

The PSO method has been proven superior in electromagnetic torque capability, which is crucial for inspection train applications. PSO produces the highest starting torque, reaching 26.3937 Nm at 0.01353 s. This method also shows the highest torque surge when the train passes through a curve, reaching 4.92347 Nm. The larger compensation torque indicates a more effective controller ability in responding to and handling sudden mechanical load disturbances.

Although ABC provides the fastest rise time under no-load conditions at 0.244482 s, the performance of PSO shows superior endurance under load variations. PSO has the shortest recovery time back to the reference speed after a speed drop caused by a curve (15.8638 s at the first curve). This fast recovery time implies better settling time and higher robustness against load disturbances, which are the main objectives of optimization. The Hand Tuning (HT) method shows suboptimal overshoot performance, where the achieved speed tends to exceed the reference speed at each curve, which is an indication of poor stability.

The Particle Swarm Optimization (PSO) tuning method is the most effective for optimizing BLDC motor speed control in inspection train applications. The combination of the highest electromagnetic torque and the fastest speed recovery capability indicates that PSO produces the most optimal K_p and K_i parameters to ensure good dynamic response and superior resistance to load disturbances that occur in rail operations.

ACKNOWLEDGMENT

This research was supported by funding from the **BIMA Grant Program (Research and Community Service Management Information System)**. The authors gratefully acknowledge the support provided.

REFERENCES

1. J.-L. Hu, Y. Li, and J.-C. Chew, "Industry 5.0 and Human-Centered Energy System: A Comprehensive Review with Socio-Economic Viewpoints," *Energies*, vol. 18, no. 9, p. 2345, May 2025, doi: 10.3390/en18092345.
2. J. M. Rožanec *et al.*, "Human-centric artificial intelligence architecture for industry 5.0 applications," *Int. J. Prod. Res.*, vol. 61, no. 20, pp. 6847–6872, Oct. 2023, doi: 10.1080/00207543.2022.2138611.
3. S. Sarp, M. Kuzlu, V. Jovanovic, Z. Polat, and O. Guler, "Digitalization of railway transportation through AI-powered services: digital twin trains," *Eur. Transp. Res. Rev.*, vol. 16, no. 1, p. 58, Oct. 2024, doi: 10.1186/s12544-024-00679-5.
4. S. P. Patil, A. S., B. S., S. M., and D. K., "REVIEW ON PAST, PRESENT, AND FUTURE OF RAILWAY SYSTEM," vol. 12, no. 05, 2025.
5. S. Ait Ahmed, Y. Gagou, B. Jonckheere, and R. Bouzerar, "Electrical capturing system for train supplying and involving parameters," *OAJ Mater. Devices*, vol. 6, no. 1, pp. 1127-1-1127–8, Nov. 2022, doi: 10.23647/ca.md20221127.
6. A. Prasanthi, H. Shareef, R. Errouissi, M. Asna, and A. Mohamed, "Hybridization of battery and ultracapacitor for electric vehicle application with dynamic energy management and non-linear state feedback controller," *Energy Convers. Manag. X*, vol. 15, p. 100266, Aug. 2022, doi: 10.1016/j.ecmx.2022.100266.
7. O. A. Filina *et al.*, "Increasing the Efficiency of Diagnostics in the Brush-Commutator Assembly of a Direct Current Electric Motor," *Energies*, vol. 17, no. 1, p. 17, Dec. 2023, doi: 10.3390/en17010017.
8. X. Li, H. Yuan, W. Chen, L. Yu, and X. Gu, "Commutation Torque Ripple Reduction Strategy of Brushless DC Motor Drives Based on Boosting Voltage of DC-Link Small Capacitor," *Micromachines*, vol. 13, no. 2, p. 226, Jan. 2022, doi: 10.3390/mi13020226.
9. S. Muralidharan, B. T., P. Kumar K.S, and A. C., "Performance analysis of controllers in BLDC motor," *E3S Web Conf.*, vol. 387, p. 01001, 2023, doi: 10.1051/e3sconf/202338701001.
10. R. Batra, G. Ezhilarasan, D. Kumar, and S. K. Jain, "Advances in BLDC motor control: A thorough examination of torque ripple reduction and speed regulation techniques," *Multidiscip. Rev.*, vol. 6, p. 2023ss053, Apr. 2024, doi: 10.31893/multirev.2023ss053.
11. O. E. M. Youssef, M. G. Hussien, and A. E.-W. Hassan, "A new simplified sensorless direct stator field-oriented control of induction motor drives," *Front. Energy Res.*, vol. 10, p. 961529, Sep. 2022, doi: 10.3389/fenrg.2022.961529.
12. M. Kumar, S. Tiwari, V. Kumar, S. J. Sampathi, and R. Kumar Jarial, "Implementation of Field-Oriented Control (FOC) Algorithm for Brushless DC (BLDC) Motor Speed Regulation," in *2023 Second IEEE International Conference on Measurement, Instrumentation, Control and Automation (ICMICA)*, Kurukshetra, India: IEEE, May 2024, pp. 1–6. doi: 10.1109/ICMICA61068.2024.10732537.

13. W. Pribadi, D. A. Wicaksono, R. Y. Wicaksono, R. G. Putra, M. S. Asbullah, and R. M. Sandy, “Grey Wolf Optimizer (GWO) For Field Oriented Control Traction Motor Of Light Rail Transit Jabodebek Train,” 2025.
14. [14]M. F. Kethiri, O. Charrouf, A. Betka, M. Salman, and C. Boccaletti, “Minimizing Power Losses in BLDC Motor Drives Through Adaptive Flux Control: A Real-Time Experimental Study,” *Actuators*, vol. 14, no. 8, p. 395, Aug. 2025, doi: 10.3390/act14080395.
15. A. I. Abouseda, R. O. Doruk, and A. Amini, “Parameter Identification and Speed Control of a Small-Scale BLDC Motor: Experimental Validation and Real-Time PI Control with Low-Pass Filtering,” *Machines*, vol. 13, no. 8, p. 656, Jul. 2025, doi: 10.3390/machines13080656.
16. P. Bhandari *et al.*, “Application of Particle Swarm Optimization (PSO) Algorithm for PID Parameter Tuning in Speed Control of Brushless DC (BLDC) Motor,” *J. Phys. Conf. Ser.*, vol. 2570, no. 1, p. 012018, Aug. 2023, doi: 10.1088/1742-6596/2570/1/012018.
17. K. Vanchinathan and N. Selvaganesan, “Adaptive fractional order PID controller tuning for brushless DC motor using Artificial Bee Colony algorithm,” *Results Control Optim.*, vol. 4, p. 100032, Sep. 2021, doi: 10.1016/j.rico.2021.100032.
18. Q. Mohammed, N. Desik, and Y. Narri, “Design and implementation of an intelligent multi modular joint (MMJ)-brain controller: application to aircraft and brushless DC (BLDC) systems,” *Int. J. Dyn. Control*, vol. 9, pp. 1–19, Dec. 2021, doi: 10.1007/s40435-021-00773-9.
19. E. Widya Suseno and A. Ma’arif, “Tuning of PID Controller Parameters with Genetic Algorithm Method on DC Motor,” *Int. J. Robot. Control Syst.*, vol. 1, no. 1, pp. 41–53, Feb. 2021, doi: 10.31763/ijrcs.v1i1.249.
20. S. R. Kamde and M. S. Morey, “Adaptive Speed Control of Permanent Magnet Brushless DC Motor by Implementing PSO Algorithm,” vol. 16, no. 6, 2021.
21. I. Anshory, D. Hadidjaja, and I. Sulistiyowati, “Measurement, Modeling, and Optimization Speed Control of BLDC Motor Using Fuzzy-PSO Based Algorithm,” *J. Electr. Technol. UMY*, vol. 5, no. 1, pp. 17–25, Jul. 2021, doi: 10.18196/jet.v5i1.12113.
22. K. P. Sanoj and V. Dhanya Ram, “Optimal PID Controller Tuning for Multivariable Unstable Systems by Minimizing ITAE Criteria,” *IFAC-Pap.*, vol. 57, pp. 391–396, 2024, doi: 10.1016/j.ifacol.2024.05.067.